

Appendix B $\tau \rightarrow \pi + X$ Results and Detector Optimisation

Chapter 8 has shown that the $\tau \rightarrow \pi + X$ analysis is possible in MINOS. The purpose of this appendix is to investigate how the sensitivity of the analysis changes as the major parameters of the detector are varied. These results were used, along with other considerations, to decide the optimum detector parameters for the MINOS near and far detectors in September 1997.

The following variables have been investigated to determine their effect on the $\tau \rightarrow \pi + X$ analysis:

- 2 and 4 cm plate thickness;
- 2 and 4 cm transverse cells;
- 1D versus 2D readout;
- liquid scintillator (FLS) and aluminium proportional tube (APT) active detector elements;
- application of a pulse height threshold to the data in order to combat detector noise;
- using pulse height information instead of counting the number of hits.

Detector configurations

The analysis in Chapter 8 uses a two samples of simulated events that were generated with 2 cm steel plates and 2 cm pitch liquid scintillator active detector cells. These samples contain 51577 ν_μ events with no oscillations and 17794 ν_τ CC events with saturated oscillations. They correspond to exposures of 12.5 and 37.2 kiloton years¹⁵ respectively. The configuration of 2 cm steel with 4 cm pitch cells is simulated by ganging together adjacent cells of the 2 cm steel, 2 cm pitch events. These two configurations are therefore not independent.

Two additional Monte Carlo samples were generated to study the performance of the $\tau \rightarrow \pi + X$ test in 4 cm steel. The signal sample consisted of 24539 ν_τ CC events (an exposure of 51.3 kiloton years) and the background sample contained 27058 ν_μ NC and CC interactions (an exposure of 6.6 kiloton years). The 4 cm steel files have two crossed scintillator readout planes per passive steel plane (i.e. two co-ordinates per steel plane). Since the effective nuclear interaction length in this configuration is the same as the configuration of 2 cm steel and 2 cm cells, the applied cuts (including EVLENGTH and STARHITS) are the same.

Simulated events have also been generated with the response function of the aluminium proportional tube (APT) active detectors. Samples consisting of 28490 ν_μ events (an exposure of 6.9 kiloton years) and 15238 ν_τ CC events (an exposure of 31.8 kiloton years) were generated in 4 cm steel with two-dimensional readout (cathode strips and anode wires). No data was available for 2 cm steel.

¹⁵ The ν_τ exposure corresponds to $\nu_\mu \rightarrow \nu_\tau$ oscillations with $\sin^2 2\theta = 1$ and large Δm^2 .

Figure B.1 shows distributions of pulse height for wires and strips from a sample of 100 ν_μ events in 4 cm steel with APT active detectors. There is clear evidence of pulse sharing on the strips. A muon passing through a strip generally induces a signal on the two adjacent strips. These extra hits will affect many of the cuts used in the $\tau \rightarrow \pi + X$ analysis so they are eliminated by requiring that the pulse height recorded on the strips and wires is greater than 0.005 (equivalent to 0.6 m.i.ps). One-dimensional readout is simulated by discarding the strip readout and using only the wire information.

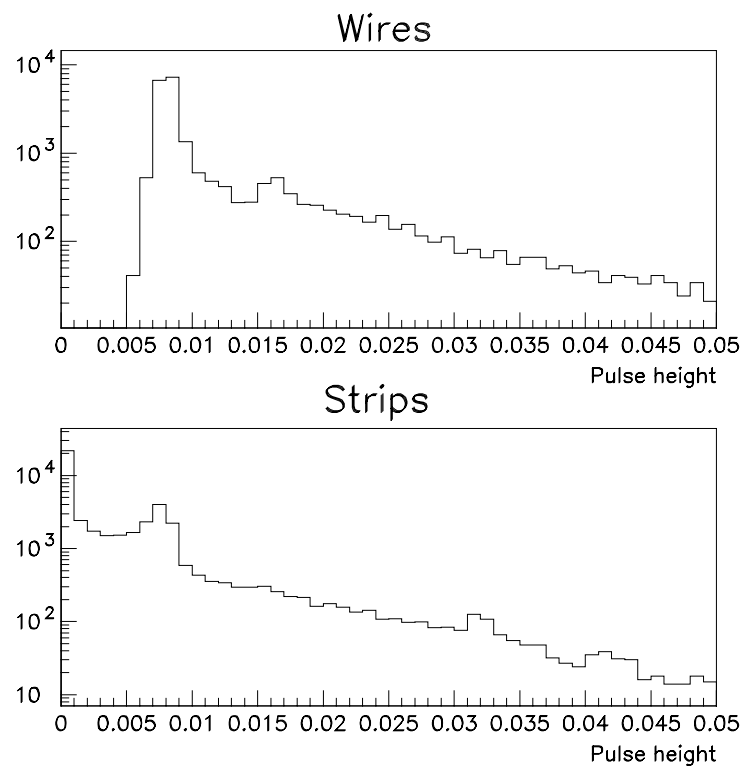


Figure B.1 – Pulse height distributions for 100 simulated ν_μ CC and NC events with APT active detectors. The top plot shows the pulse height distribution from the wire readout, and the bottom plot is for strip readout. A cut on the pulse height of 0.005 eliminates much of the pulse sharing on the strips.

Comparison between FLS and APT

The aim of this section is to compare the results of the $\tau \rightarrow \pi + X$ analysis in APT and FLS active detectors over a range of steel thickness and transverse cell size. The relative merits of the two technologies are the following:

1. APTs can, in principle, provide better transverse resolution than FLS detectors with the same transverse pitch by analysing the pulse heights induced on adjacent strips. Pulse sharing is eliminated in this analysis because it affects the `BARREL` and `FLIGHT` cuts and the Hough transform. The effect of improved transverse resolution is, however, studied in general in this Appendix to discover whether or not it is beneficial to the $\tau \rightarrow \pi + X$ analysis.
2. Scintillator based detectors provide better energy resolution than gas detectors (by a factor of 1.5) because they sample a larger fraction of the hadron shower (the cross-section for low energy neutron/proton scattering in the scintillating medium is higher than that in gas). This is the reason why simulated data with FLS active detectors produce approximately twice the number of hits per GeV as APT detectors with the same detector configuration, as shown in Table B.1

Configuration	Hits/GeV	Pulse height/GeV	1 m.i.p response
FLS22	19.3	549	22.5
FLS24	15.8	549	22.5
FLS42	19.5	541	22.5
FLS44	15.9	541	22.5
FLS42 (1D)	9.8	274	22.7
FLS44 (1D)	8.0	274	22.7
APT42	9.3	0.13	0.0178
APT44	8.3	0.13	0.0178
APT42 (1D)	4.6	0.094	0.0109
APT44 (1D)	3.7	0.094	0.0109

Table B.1 – Detector response for various configurations of active and passive detector. The first column lists the configuration, following the format: active detector (FLS or APT); steel thickness (cm); transverse cell size (cm); (readout). The second column lists the mean number of hits per GeV for NC events. The third column lists the mean pulse height per GeV for NC events and the final column lists the mean pulse height per plane (in arbitrary units) produced by a minimum ionising particle. These arbitrary units are different for the APT and FLS configurations.

Four variations of the cuts are applied to the data samples.

1. events are selected using BARREL and FLIGHT variables. The number of STARHITS must be equivalent to 2 GeV of visible energy or more. Column 2 of Table B.1 lists the number of hits/GeV for each detector configuration;
2. events are selected using BARREL and FLIGHT variables as above but the energy of the star is estimated from the summed pulse height in the FLIGHT region. Column 3 of Table B.1 lists the summed pulse height/GeV for each configuration. The energy of the star must be greater than 2 GeV. Figure B.2 shows distributions of the star energy for signal and background events, calculated from hits and pulse height information, for the FLS22 configuration;

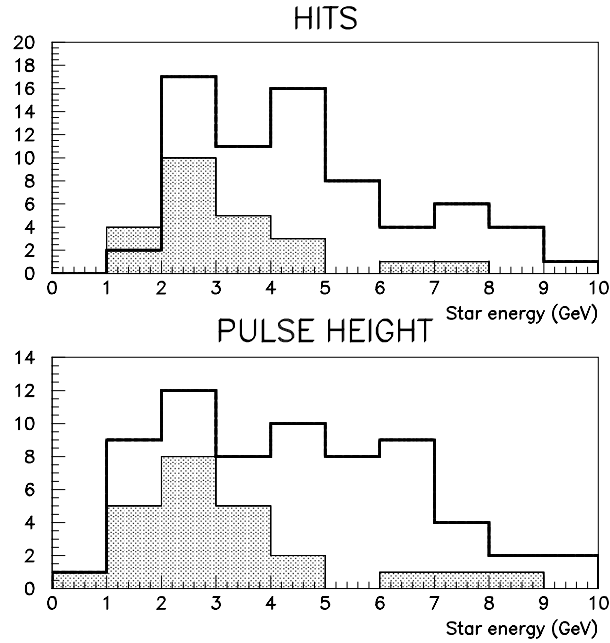


Figure B.2 – The energy of the hadronic star estimated from counting the number of hits (top plot) and from summing the total pulse height (bottom plot) in the FLIGHT region. The open histograms are for ν_τ events passing all cuts and the shaded histograms are for ν_μ events.

3. BARREL and FLIGHT variables are not used to select events. Pulse height information is used to construct the number of mips per plane in the BARREL and FLIGHT regions. Column 4 of Table B.1 shows the mean pulse height per plane produced by a minimum ionising particle. The number of mips per plane in the BARREL region is the summed pulse height per plane in the first half of the event divided by the mean pulse height per plane produced by a mip. Figure B.3 shows BARREL versus FLIGHT distributions for signal and background events in the FLS22 configuration above the corresponding distributions in BARREL MIPS versus FLIGHT MIPS space. The following cuts are applied in mip space:

- BARREL MIPS < 5;

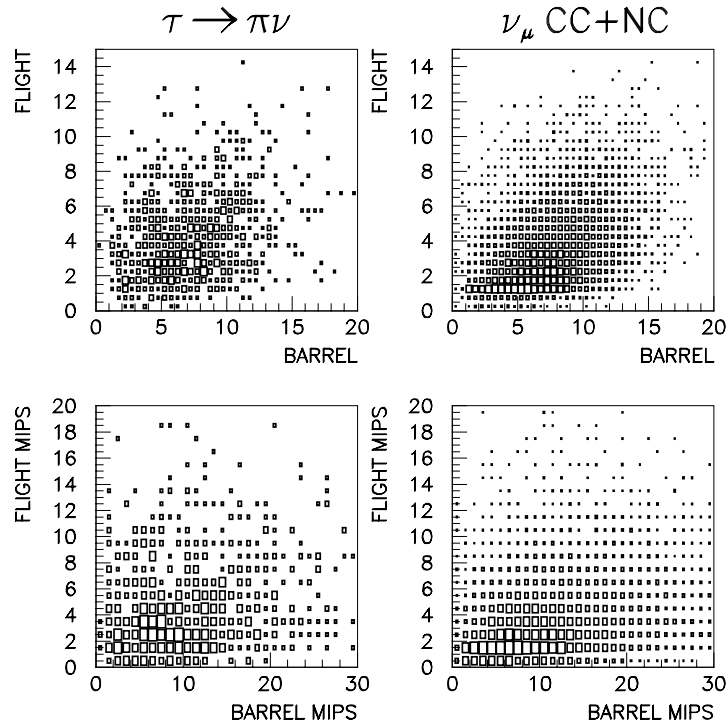


Figure B.3 - Track→star event selection in 2 cm steel, 2 cm cells with FLS active detectors. The left-hand plots show distributions for $\tau \rightarrow \pi\nu$ events and the right hand plots show distributions for ν_μ NC and CC events. The top plots are distributions of BARREL and FLIGHT, which are defined using hit information. The bottom two plots are distributions of the number of minimum ionising particles per plane in the BARREL and FLIGHT regions, which are defined using pulse height information. Track→star events lie in the top left hand sectors of each plot.

- FLIGHT MIPS > 1.5;
- FLIGHT MIPS > 1.17 × BARREL MIPS – 0.84.

The energy of the star, as estimated by pulse height, is required to be greater than 2 GeV;

4. a minimal set of cuts is applied to the data. Figure 8.13 in Chapter 8 shows that some of the cuts have a large effect on signal/background selection efficiency

whereas others have only a small effect. Only those cuts which have a large effect are applied to the data. These cuts are:

- $20 < \text{EVLLENGTH} < 60$;
- BARREL MIPS and FLIGHT MIPS cuts;
- $\text{RMS75} < 10$;
- $\cos \theta_z > 0.95$.

Event selection: hits, Star energy: hits

Figure B.4 shows the signal expected for the $\tau \rightarrow \pi + X$ test in a two-year run of MINOS, assuming $\nu_\mu \rightarrow \nu_\tau$ oscillations with $\sin^2(2\theta) = 1$ and large Δm^2 , in a number of detector configurations. Event selection and star energies are based on hits information. The left-hand plot, which shows the signal/noise ratio (signal/ $\sqrt{\text{background}}$) that could be obtained in each configuration, indicates that FLS active detectors (filled circles) and APT detectors (open circles) produce very similar numbers. The signal/noise ratio is not a strong function of either steel thickness or transverse granularity. One dimensional readout with 4 cm steel produces a smaller signal/noise ratio than the other configurations.

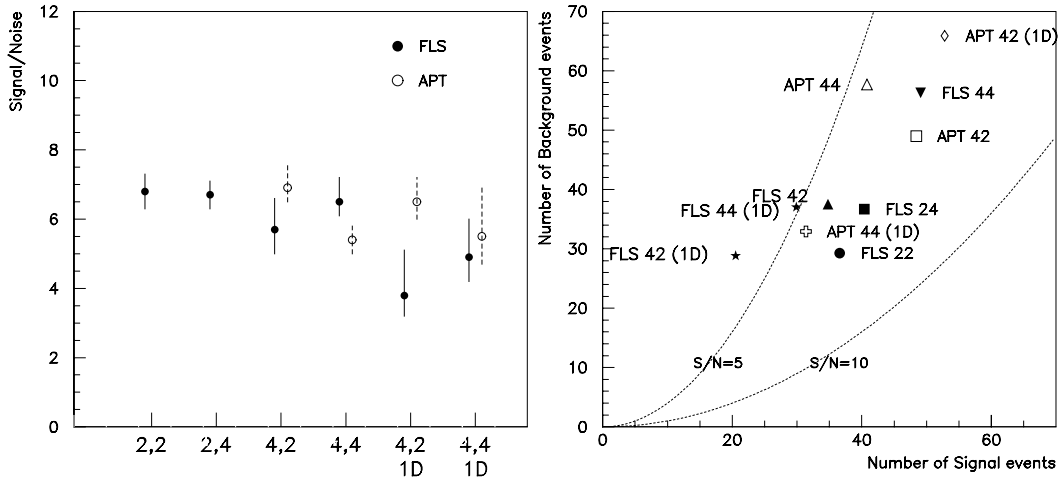


Figure B.4 - $\tau \rightarrow \pi + X$ sensitivity for various detector configurations. Events are selected using hits and the star energy is estimated from counting the number of hits in the FLIGHT region. The leftmost plot shows the signal to noise ratio that could be obtained in a two-year run of MINOS for various configurations. The error bars are at 90% C.L. The right-hand plot shows the normalised numbers of signal and background events expected in a two-year run for all configurations. Two lines of constant signal to noise ratio are also plotted.

The right-hand plot in Figure B.4 shows the numbers of signal ν_τ CC events and background ν_μ events expected in a two-year exposure of MINOS for each detector configuration. The errors on these numbers are omitted for clarity. A line drawn from the origin to the top right-hand corner of the plot indicates a signal to background ratio of 1.0. The best signal/background ratio is obtained in 2 cm steel with 2 cm transverse granularity. In general, increasing the steel thickness, decreasing the transverse granularity and switching from 2D readout to 1D readout reduces the signal/background ratio. The left-hand plot indicates that the FLS22 and APT42 (1D) configurations have the same signal/noise ratio but the right-hand plot shows that more than double the number of background events pass the cuts in the APT42 (1D) configuration. The signal/background ratio is therefore worse than for the FLS22 configuration.

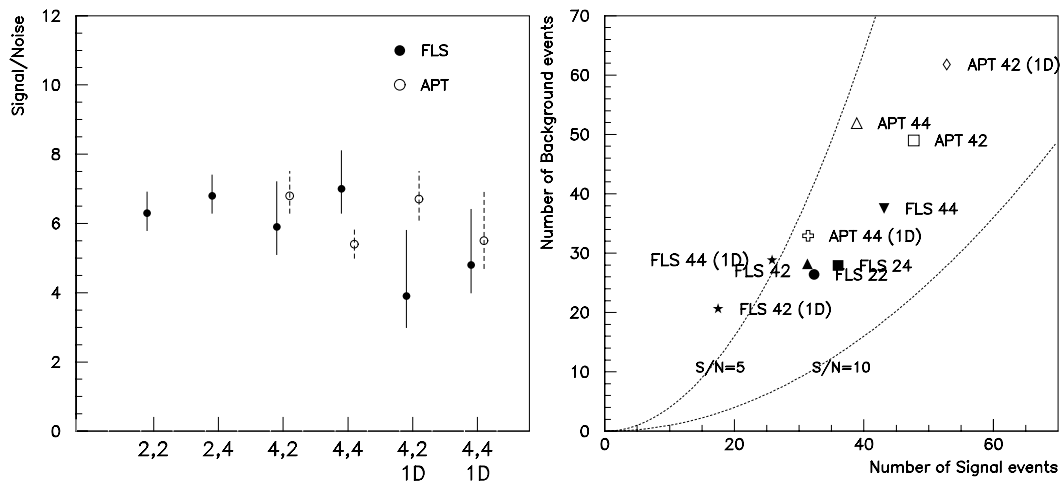


Figure B.5 - $\tau \rightarrow \pi + X$ sensitivity for various detector configurations. Events are selected using hits and the star energy is estimated from pulse height information.

Event selection: hits, Star energy: pulse height

Figure B.5 shows the signal to noise ratios and normalised numbers of signal and background events expected if pulse height is used to estimate the energy of the star. The signal/noise ratios obtained in each configuration are similar to those of Figure B.4. Four centimetre steel with 1D readout produces lower signal/noise ratios than the other configurations.

The effect of using pulse height to estimate the energy of the star instead of using hit information can be seen by comparing the right-hand plots of Figure B.4 and Figure B.5. The numbers of signal and background events passing the cuts are fewer when pulse height information is used, i.e. the absolute $\tau \rightarrow \pi + X$ selection efficiency is reduced. Pulse height information does, however, improve the signal/background ratio; more of the points have a signal/background ratio of 1.0 or better.

Event selection: pulse height, Star energy: pulse height

Figure B.6 shows the signal/noise and normalised numbers of signal and background events expected if the events are selected by cutting on the number of mips per plane in the BARREL and FLIGHT regions and pulse height is used to estimate the energy of the star. The left-hand plot shows the same features as the previous two figures although the absolute level of signal/noise is reduced somewhat. This is purely an acceptance issue; a cut of 5 mips/plane is not the same as 5 hits/plane since two particles passing through one cell will produce a pulse height signal equivalent to two mips but only one hit. The acceptances for FLS and APT active detectors will be slightly different since the 1 mip peak is wider in the APT simulation than in the FLS (30% versus 10%). The plot indicates that 4 cm steel with 1D readout is again inferior to the other configurations but the points are consistent with a constant value of signal/noise due to the large statistical errors.

The right-hand plot of Figure B.6 shows that the absolute selection efficiency is

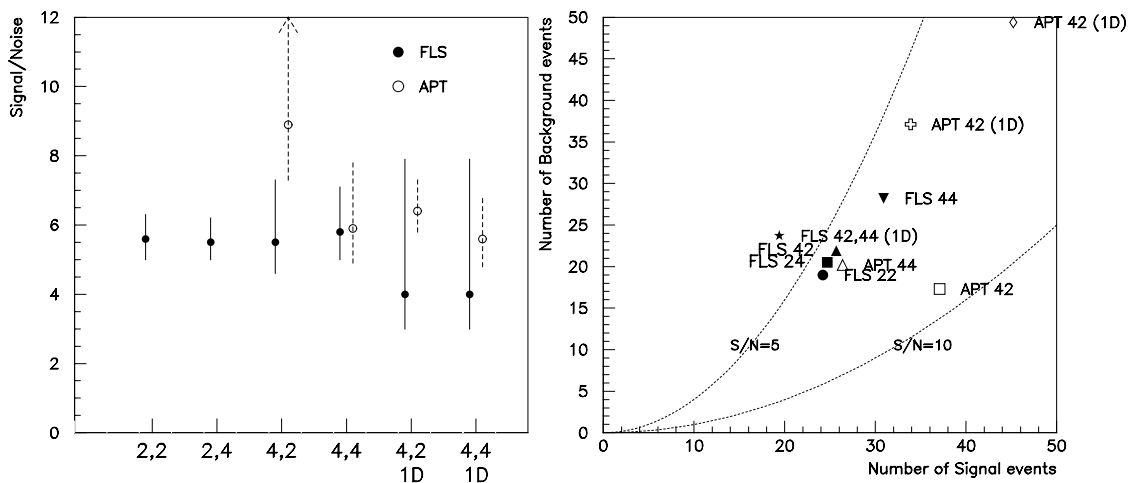


Figure B.6 - $\tau \rightarrow \pi + X$ sensitivity for various detector configurations. Events are selected using pulse height and the star energy is estimated from pulse height information.

reduced when pulse height is used to select events (note the different scale to the other plots). The benefit of using pulse height is that almost all the configurations produce a signal/background ratio of 1.0 or greater. In Figure B.4, there are significant differences in acceptance for closely similar configurations. The points FLS22 and FLS24 are separated in Figure B.4; degrading the transverse resolution increases the acceptance but reduces the signal/background ratio since there is a higher probability that two particles will pass through the same cell. When pulse height is used to select events, it is possible to resolve mips passing through the same cell and the acceptances for FLS22 and FLS24 are practically identical in Figure B.6.

Event selection: pulse height, minimal cuts

Figure B.7 shows the signal/noise ratio and normalised numbers of signal and background events expected if events are selected using pulse height information and only cuts that have a large effect on the signal/background ratio are applied. Comparing Figure B.7 to Figure B.6 shows that the signal/noise ratio is increased when only the minimal cuts are applied. The smaller statistical errors in Figure B.7 show more clearly the loss in sensitivity for the configurations with 4 cm steel and 1D readout. The FLS data is slightly worse than the APT data for these configurations.

The right-hand plot of Figure B.7 shows that the acceptance is indeed larger when the minimal cuts are applied although, in contrast to Figure B.6, most of the configurations produce a signal/background ratio of less than 1.0. It is interesting to note that the acceptance for the APT configurations does not change significantly between Figure B.6 and Figure B.7 whereas the FLS configurations show a marked increase in acceptance. This indicates that the cuts which have been applied in Figure B.6 but not in Figure B.7 are cutting on properties of the events that are more common to FLS data than APT data. One example of this is the presence of ‘scattered hits’ in FLS events, due to neutrons scattering off hydrogen in the scintillator, which are not present in the APT data.

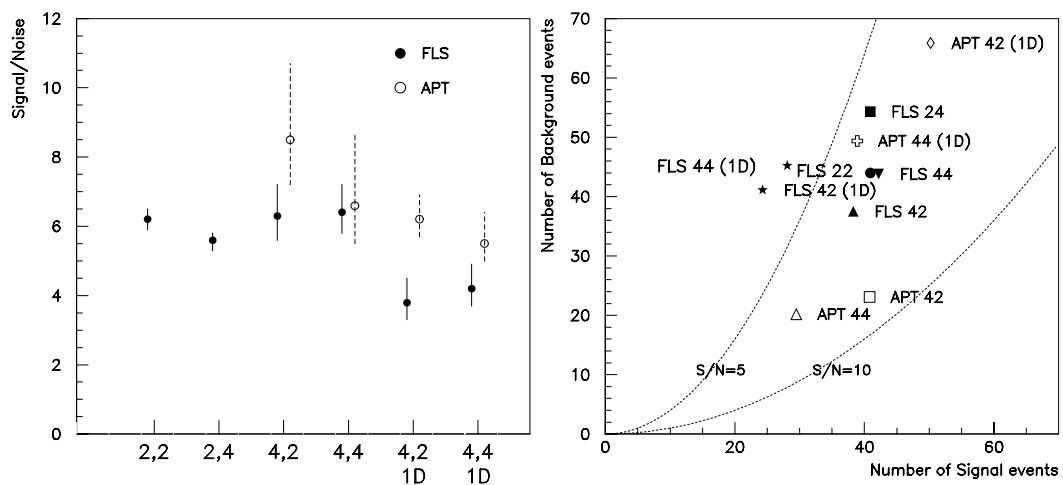


Figure B.7 - $\tau \rightarrow \pi + X$ sensitivity for various detector configurations. Events are selected using pulse height and only cuts that have a large effect on signal/background selection efficiency are applied.

Sensitivity to neutrino oscillations

The $\tau \rightarrow \pi + X$ analysis, which relies on the observation of a high momentum pion track that subsequently creates an energetic hadron shower, is clearly energy dependent. The analysis will be relatively inefficient at low neutrino energy, reducing the sensitivity of the analysis to oscillations with low Δm^2 . Figure B.8 shows the low Δm^2 segment of six limit plots for different FLS detector configurations (the APT limits are practically identical and are not plotted). The low Δm^2 behaviour of the 6 limit plots is very similar.

The sensitivity of the $\tau \rightarrow \pi + X$ test to the Kamiokande parameters can be estimated by reading off the limits on $\sin^2(2\theta)$ shown in Figure B.8. At $\Delta m^2 = 0.01 \text{ eV}^2$ the $\tau \rightarrow \pi + X$ analysis is predicted to set a limit on $\sin^2(2\theta)$ of between 0.275 and 0.375,

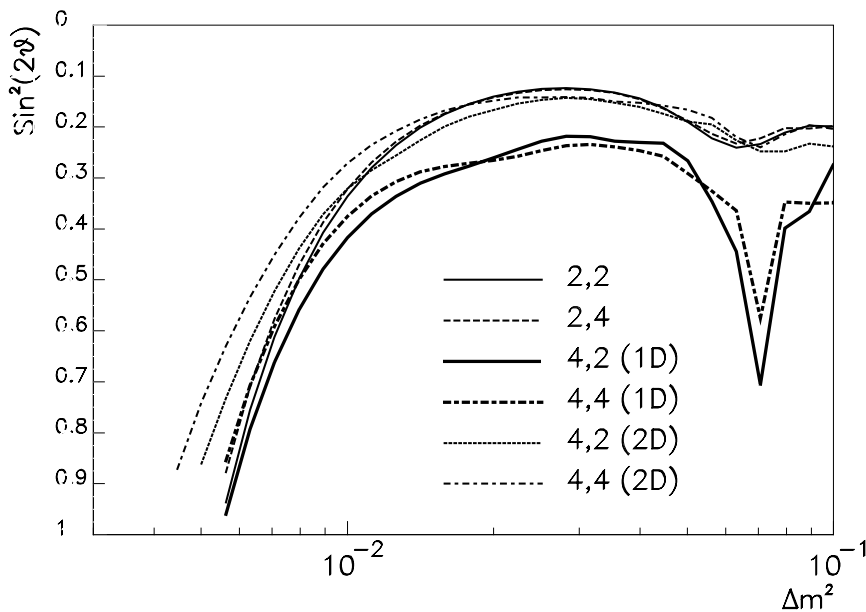


Figure B.8 – Predicted 90% confidence limits at low Δm^2 in the mode $\nu_\mu \rightarrow \nu_\tau$ for a 2 year run in the WBB for 6 detector configurations. The thin solid line shows the limit that can be set in 2 cm steel with 2 cm cells.

depending on the detector configuration. The significance of the oscillation signal, $signal / \sqrt{background}$, is related to $\sin^2(2\theta)_{\min}$ by:

$$S / \sqrt{B} = 1.29 / \sin^2(2\theta)_{\min}. \quad (\text{B.1})$$

This equation yields a significance of between 3.4 and 4.7 standard deviations for $\Delta m^2 = 0.01 \text{ eV}^2$

Conclusions for detector optimisation

Transverse granularity

The sensitivity of the $\tau \rightarrow \pi + X$ test to neutrino oscillations is not affected when the transverse cell size is increased from 2 cm to 4 cm because the signal/noise ratio is the same in both configurations. If hits are used to select events then there is an increase in acceptance when the transverse cell size is increased since there is a higher probability for two particles to pass through the same cell. The acceptance for 2 cm and 4 cm cells is the same if pulse height is used to select events.

Longitudinal granularity

The sensitivity of the $\tau \rightarrow \pi + X$ test to neutrino oscillations is not affected when the steel thickness is increased from 2 cm (with 1D readout) to 4 cm (with 2D readout). For liquid scintillator active detectors, these two configurations have the same effective interaction length so this result is not surprising. Comparing the results of 4 cm steel with 1D readout to 2 cm steel with 1D readout shows a reduction in sensitivity to oscillations.

1D readout versus 2D readout

One-dimensional readout with 4 cm steel plates produces lower signal/noise and signal/background ratios than 2D readout with the same steel thickness. This is because there are fewer hits per GeV for 1D readout, producing a poorer estimate of the star energy, and the number of hits in a track is reduced by a factor of two, resulting in a poorer track finding efficiency.

Pulse height versus hits

Pulse height can be used to select events on the basis of the number of hits per plane in the BARREL and FLIGHT regions and to estimate the energy of the star. The use of pulse height instead of counting the number of hits reduces the selection efficiency somewhat but improves the signal/background ratio. This is because multiple mip crossings can be resolved in a single cell.

APT versus FLS

APT data and FLS data produce similar values of signal/noise in all configurations with 4 cm steel (no APT data was available in 2 cm steel). The two technologies produce somewhat different acceptances because the response to a mip is different (the APT simulations show a wider mip peak) and the APT data has fewer hits/GeV for neutral current events than the FLS data. The sensitivity to neutrino oscillations, however, is the same in both active detectors.

Optimal detector configurations for $\tau \rightarrow \pi + X$

The absolute efficiency of the $\tau \rightarrow \pi + X$ test for $\tau \rightarrow \pi\nu$ events is small (2.2%) and only a few tens of track \rightarrow star events are expected in a two year run for maximal neutrino

oscillations at large Δm^2 . The test is therefore limited by statistics and is only believable if it produces a large signal/noise ratio (greater than 5) and a good signal/background ratio (about 1.0 or better). Given these conditions, the best detector for $\tau \rightarrow \pi + X$ is fine-grained (2 cm steel with 2 cm transverse pitch). Configurations with 4 cm transverse pitch and/or 4 cm steel (with 2D readout) produce the same signal to noise ratio as 2 cm steel with 2 cm transverse pitch, albeit with a slightly worse signal/background ratio. 4 cm steel with 1D readout produces a low signal/noise ratio and a poor signal/background ratio, therefore it is not favourable to this analysis. Good pulse height capabilities can help to increase the signal/background ratio, although there appears to be no advantage for scintillator over gas detectors or *vice versa* when pulse height information is used.